Atomistic simulation of stacking fault formation in bcc iron

Anna Machová†, Glenn E Beltz‡ and Margherita Chang‡

- † Institute of Thermomechanics AS CR, Dolejskova 5, 18200 Prague 8, CZ
- ‡ Department of Mechanical and Environmental Engineering, University of California, Santa Barbara, CA 93106-5070, USA

Received 11 March 1999, accepted for publication 26 July 1999

Abstract. We present large scale atomistic simulations of crack growth in iron under quasistatic loading in mode I. We show that long cracks display a brittle character of extension, while the growth of smaller cracks is accompanied by emission of partial dislocations from the crack tip and subsequent transformation of the stacking faults behind the dislocations to multilayer twins. The competing shear processes at a crack tip are characterized in terms of the relative sliding of up to four adjacent atomic planes emanating from the crack tip region. The results are in agreement with a global energy balance derived from perfect samples, and with experimental observations that twinning and fracture are cooperating processes under sufficiently large quasistatic loading at low temperatures.

1. Introduction

Experimental studies reviewed by Ogawa [1] show that twins in a body-centred cubic (bcc) crystal may form concomitantly with partial dislocations in the {112} slip system and that twinning and fracture at low temperatures or at high strain rate are cooperating processes in bcc iron or Fe–Si alloys. For that reason, the stress required for twinning in bcc crystals is often regarded as a fracture stress, both in theoretical [2] and experimental studies [1]. Recent atomistic studies of a microcrack in bcc iron under impact loading [3] show that under high strain rates, twin formation at the crack tip accompanies crack extension, which support the aforementioned experimental findings.

Vitek [4] studied the generation of stacking faults (SFs) and multilayer twins on the {112} planes in perfect bcc crystals under static conditions, using various pair potentials, and concluded that intrinsic SFs are unstable, while extrinsic three and four layer SFs (3SF and 4SF), or multilayer twins may be stable in bcc. It was also shown that the energy barrier between 3SF, 4SF and the twins in the (111){112} slip systems is small. Subsequently, Bristowe *et al* [5] showed basically similar results, but underscored the need for realistic modelling of atomic relaxation normal to the plane undergoing the shear process. These observations lead to an obvious conflict when trying to understand the fracture behaviour of bcc iron in terms of a simple competition between crack extension and dislocation nucleation, as suggested by Rice and Thomson [6] and Rice [7]—for one not only must consider the possibility of full dislocation nucleation, but additionally, other potential outcomes which include the emission of one or more partial dislocations, followed by an intrinsic or extrinsic (additional layer) SF.

More recently, twins in the slip systems $\langle 111 \rangle \{112\}$ for the same crack orientation used in this study, under quasistatic loading, were observed in simulation studies using other potentials for bcc iron, for example in studies by Mullins [8] and Cheung and Yip [9]. Generation of SFs

in bcc iron at 0 K under static conditions has also been observed in simulations by Shastry and Farkas [10], albeit in a different crack orientation. More recently, twin formation in bcc iron under static loading and a plastic instability caused by twining in the perfect crystal was reported in atomistic simulations by Hu *et al* [11] for the same crystal orientation as used in this study.

This paper examines nanoscopic processes at a crack tip under quasistatic loading, as well as the formation of SFs and twins in perfect crystals under static conditions at 0 K. Our studies of shear processes in the $\langle 111 \rangle \{112\}$ slip systems in perfect crystals are based on a global energy balance in sufficiently large samples, similar to Vitek [4]. We use an N-body (GA) potential presented by Machová and Ackland [3] and Ackland $et\ al\ [12]$. Our main goal is to attempt to understand shear processes at a crack tip in terms of a generalized Peierls—Nabarro-like slipping of adjacent planes, much in the spirit of Rice's analysis [7] of single dislocation emission at a crack tip in materials with less complex faulting behaviour and valid for relatively planar dislocation cores.

For the studies of brittle–ductile behaviour at the crack tip loaded in mode I, we use molecular dynamic (MD) simulations with the same border conditions and crack orientation as described in a recent paper [3]. The slip system $\langle 111 \rangle \{112\}$ is inclined with respect to the crack front at an angle $\theta \approx 35^{\circ}$. Unlike [3], we present MD simulations under quasistatic loading, accompanied by calculations of the interplanar stresses and of local energies in the slip system $\langle 111 \rangle \{112\}$ on the atomistic level.

Interplanar forces for pair potentials were introduced by Benedek *et al* [13]. The interplanar stress associated with the N-body (GA) potential of Finnis and Sinclair [14] is presented in section 3.2 of this paper, and enables quantitative analysis of the observed shear processes at the crack tip. It will be shown that the interplanar concept leads to an agreement with the global energy balance and local force balance under inhomogeneous strain distributions across an interface. Under homogeneous strain, the interplanar stresses agree with the local atomic volume stresses, defined for N-body potentials in [15, 16].

Additionally, we show that while a stable 3SF may also exist in a perfect bcc crystal for a GA potential (in agreement with Vitek [4]), the stress conditions at a loaded crack tip do not enable the stable existence of partial dislocations and of a 3SF in the slip system $\langle 111 \rangle \{112\}$. When interplanar shear stresses on interior atoms in the slip system reach the first zero point (and potential energy is a maximum), the 3SF is transformed to a multilayer twin. The transformation begins at the crack tip, where stress conditions exist similar to those at an ideal coherent twin boundary. We show that under larger applied stress, an extensive fast twin transformation may occur at the crack tip, leading to an elementary crack advance. The observed shear processes are accompanied by bond breakage in the $\langle 111 \rangle \{112\}$ slip systems for the short range GA potential [3]. The results presented in this study are not influenced by stress waves emitted after the bond breakage and subsequently reflected from the sample borders back to the crack tip.

For longer cracks, where a smaller Griffith stress is needed for brittle crack extension, some incipient shear processes are localized only in the nearest vicinity of the crack tip, and the defects disappear after crack advance. In this case, twin generation is not observed and the fracture under quasistatic loading has brittle character.

2. Atomistic simulations

2.1. Perfect samples

In order to study single or multiple faulting generically, we first consider an uncracked structure. The bcc lattice is projected on a (110) plane (as in figure 3 in [3]). Each projected atom

represents a chain of atoms in the perpendicular [110] direction. The crystal is oriented along the axes $x_1 = [\bar{1}10]$, $x_2 = [001]$, $x_3 = [110]$. The simulation domain consists of 198 atomic ($\bar{1}10$) planes in the x_1 -direction, 200 planes in the x_2 -direction, and three planes in the x_3 -direction. The small thickness in x_3 is sufficient to include the whole range of interactions in the bcc space lattice for the GA potential [3] under the plane strain conditions $\varepsilon_{33} = \varepsilon_{32} = \varepsilon_{31} = 0$ and periodic (translational) boundary conditions in x_3 . The crystal is divided into two parts along the (111) diagonal. The upper part is fixed and the lower part is gradually displaced (step by step) in the (111) direction in a prescribed manner, using a step 0.025b, where $b = \frac{a}{2}\langle 111 \rangle$ is the Burgers vector in a bcc crystal. We use the following notation: $D_1 = U_{10} = U_1 - U_0$ is the relative shear displacement between the fixed diagonal denoted by zero and the first neighbouring plane, 1, lying below the diagonal; $D_2 = U_{21} = U_2 - U_1$ is the relative shear displacement between the second (2) and the first (1) atomic plane below the diagonal, and similarly, $D_3 = U_{32} = U_3 - U_2$. The total displacement of the lower (moving) block with respect to the upper (fixed) part of the crystal is $\Delta = D_1 + D_2 + D_3 = U_{10} + U_{21} + U_{32} = U_3$, where U_3 is the displacement of the third plane below the diagonal in the $\langle 111 \rangle \{112\}$ slip system. During this rigid sliding in the $\{112\}$ planes, where the (111) slip direction lies, the total potential energy in the system is calculated as $E_{POT}(\Delta, 0) = (E_{POT}(D_1, D_2, D_3) - E_{POT}(0, 0, 0))/NA_{112}$. Here N is the number of atoms along the diagonal and A_{112} is the area per one atom in the {112} plane ($A_{112} = 2d_{110}b$, where d_{110} is the interplanar distance between neighbouring {110} planes). We distinguish three important cases:

- (i) $D_1 \neq 0$, $D_2 = 0$, $D_3 = 0$ is a block-like shear (BLS),
- (ii) $D_1 \neq 0$, $D_2 \neq 0$, $D_3 = 0$ is a two-layer stacking fault (2SF) and
- (iii) $D_1 \neq 0$, $D_2 \neq 0$, $D_3 \neq 0$ is a three-layer stacking fault (3SF).

Atomic configurations during BLS and 3SF formation are shown in figure 1. Furthermore, we examine deformation twinning, where the entire lower part of the crystal is gradually deformed along {112} planes in the {111} direction to obtain the ideal coherent twin (CT) depicted in figure 1. The processes of BLS, CT and 3SF formation are schematically shown in figure 2.

2.2. Cracked samples

We next consider a pre-existing atomically sharp central crack of length $2l_0$ embedded in an initially rectangular sample. Crack surfaces lie on (001) planes, the crack front is oriented along the $x_3 = [110]$ direction, and potential crack extension is in the $x_1 = [\bar{1}10]$ direction. The crack is loaded in mode I, i.e. the sample borders are loaded by external forces in the $x_2 = \langle 001 \rangle$ directions. Due to the symmetry of the problem, we only simulate one half of the sample in the x_1 -direction, with half crack length l_0 . The sample consists of 200 planes in the x_1 -direction, 400 atomic planes in the x_2 -direction, and three planes in the x_3 -direction—consistent with the plane strain conditions mentioned in section 2.1. Periodic boundary conditions are imposed in the x_3 -direction. Atoms lying at the left border of the sample (figure 10) are fixed in the x_1 -direction, while other atoms are free to move in x_1 and x_2 , i.e. the sample length and width are not fixed, similar to [3].

Prior to the external loading, the sample is relaxed to avoid the influence of surface relaxation on crack tip processes. Then, the sample is loaded gradually up to a level σ_A during 4000 time integration steps of magnitude 1×10^{-14} s. When the prescribed stress level is reached, the applied stress is held constant (figure 3).

Newtonian equations of motion are solved by the central difference method. Thermal atomic motion is not controlled in the system; that is, atomic velocities are not prescribed as in [3, 17, 18].

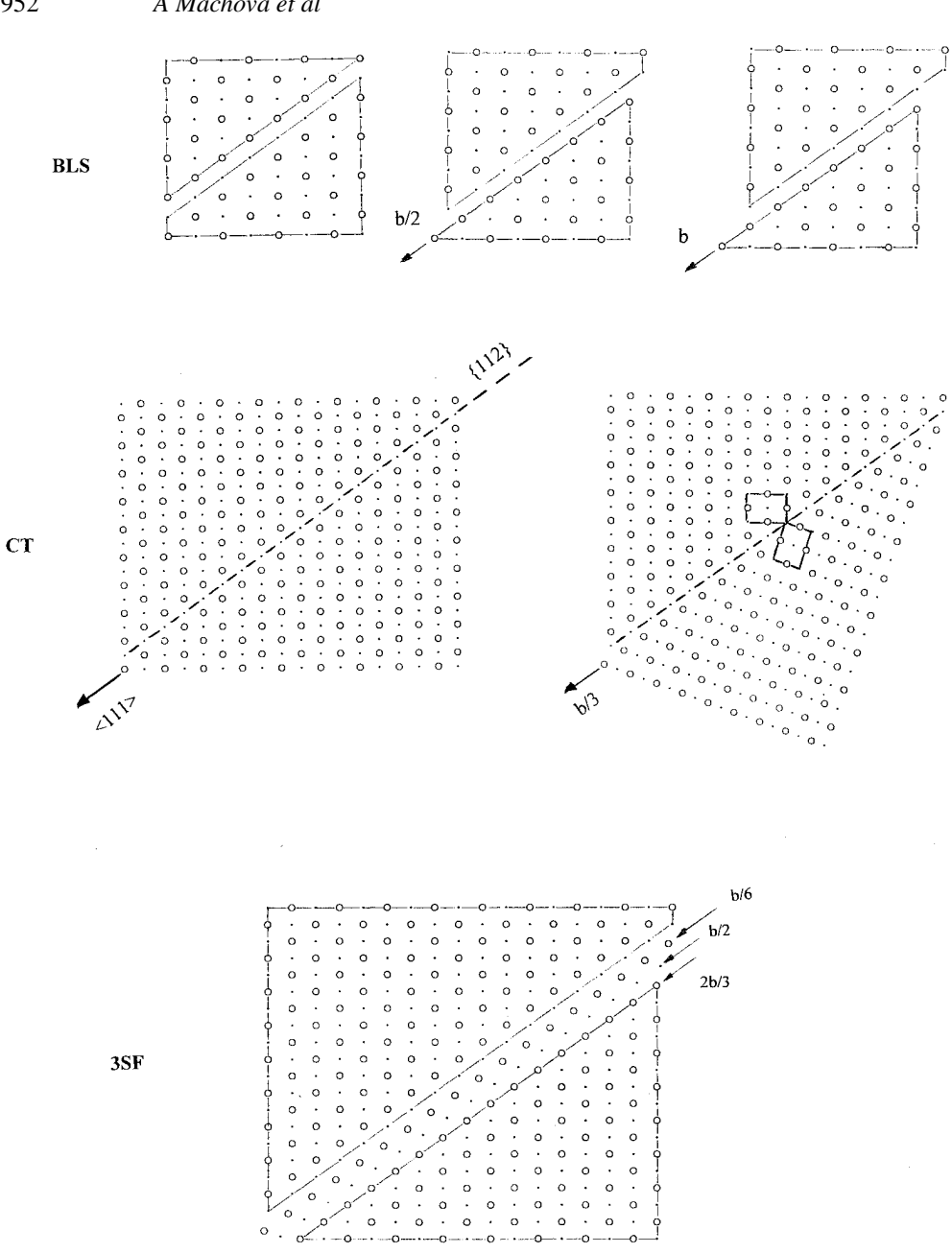


Figure 1. Atomic configuration during block-like shear (BLS), ideal coherent deformation twinning (CT) and three-layer stacking fault (3SF) formation.

During the simulations, the total potential $E_{\rm POT}$ and kinetic $E_{\rm KIN}$ energies are monitored as well as the work W_{EXT} done by external forces, to insure the energy balance $W_{\text{EXT}}(t,0) =$ $E_{POT}(t, 0) + E_{KIN}(t, 0)$ in the system at each time step. Here, $E_{POT}(t, 0) \equiv E_{POT}(t) - E_{POT}(0)$ and $E_{KIN}(0) = W_{EXT}(0) = 0$. In addition to the global balance, we also record the local kinetic and potential energies of individual atoms, and map the existing interactions in the vicinity of the crack tip, including those on the slip systems $\langle 111 \rangle \{112\}$, and also the global number of

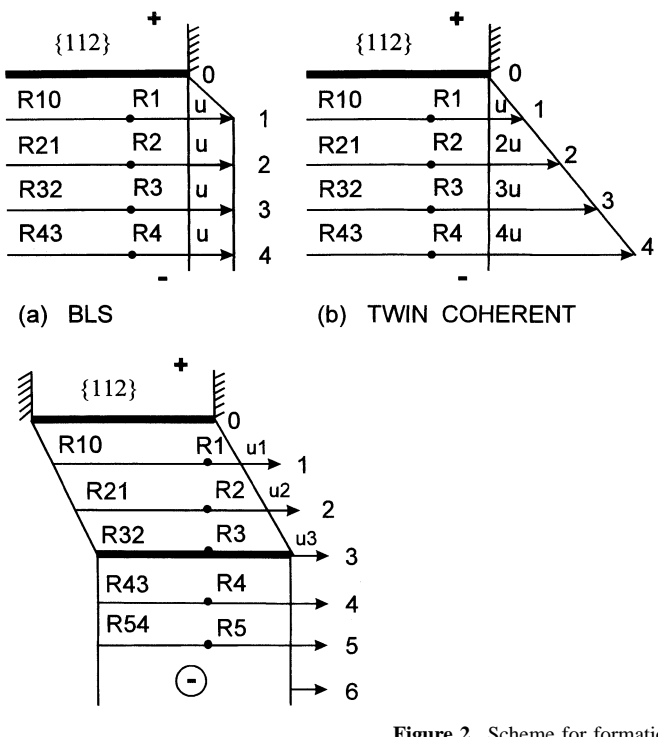
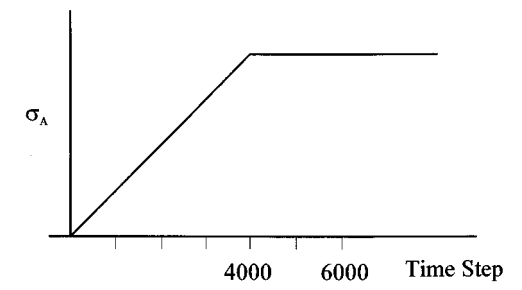


Figure 2. Scheme for formation of (*a*) BLS, (*b*) a CT and (*c*) a 3SF.



(c) 3SF

Figure 3. Applied loading sequence in MD crack simulations

existing interactions. Mapping the interactions enables us to recognize bond breakage in the slip systems and in the direction of crack propagation, i.e. to detect the onset of crack advance.

In figure 4, the atomic configuration at the crack tip and along the slip planes $0, 1, 2, 3, 4, \ldots$ is shown. The angle θ between the slip system $\langle 111 \rangle \{211\}$ and the axis of crack extension x_1 corresponds to $\tan \theta = 1/\sqrt{2}$, i.e. $\theta \approx 35^\circ$. At each time step during the loading, we record the relative shear displacements $U_{ij} = U_i - U_j$ between the individual slip planes i and j below the crack tip (notation $U_{ij}(T)$) and at interior atoms (notation U_{ij}). The monitored atomic positions are indicated in figure 4 by the full lines AC and DE. At the same atoms we also calculate the interplanar shear stresses $R_{ij}(T)$ and R_{ij} at each time step (see section 3.2).

The MD code was tested on perfect samples under uniaxial tension in the x_2 -direction and homogeneous shear along the $\langle 111 \rangle \{112\}$ slip systems, and on cracked samples loaded in mode I. Atomistic results in the elastic regime correspond well to continuum elastic anisotropic results.

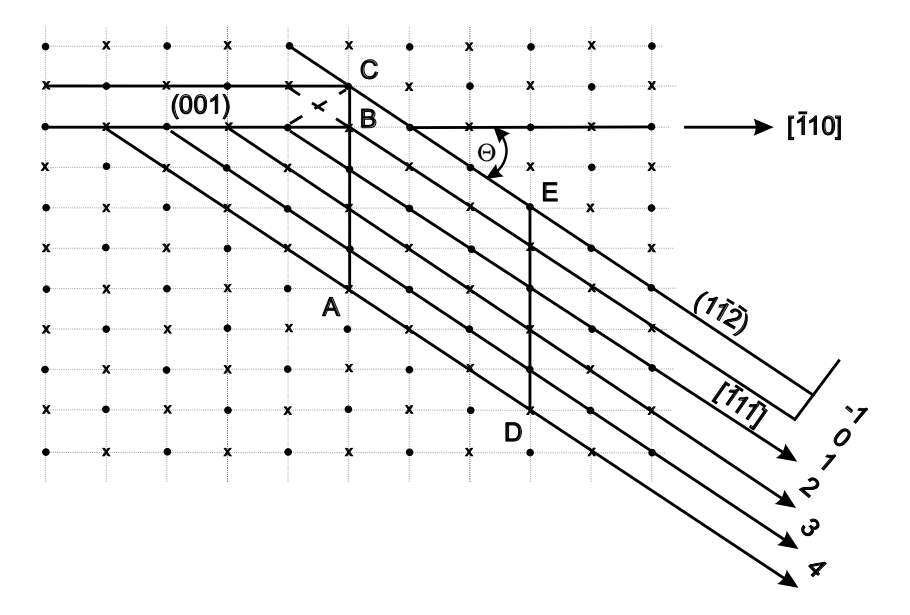


Figure 4. Atomic configuration at the crack tip and along the slip planes {112} denoted by numbers 0, 1, 2, 3, 4, etc. Vertical lines denote the region where relative shear displacements and interplanar shear stresses have been evaluated.

3. Results and discussion

The basic properties of the GA potential, such as Griffith stress intensity factor K_G , cleavage energies, elastic constants, phonon frequency spectra, wave velocities, and the theoretical stress–strain curve in the [001] direction, etc, are presented in [3, 12]. In section 3.1 we present the important characteristics of the GA potential needed for understanding brittle versus ductile behaviour.

3.1. Energy balance in perfect samples

The change in the total potential energy $E_{\rm POT}$ (in units of J m⁻²) during rigid sliding of the upper (fixed) and lower (moving) part of the crystal along the $\langle 111 \rangle \{112\}$ slip system for various values of the dimensionless shear displacements D_1/b , D_2/b , and D_3/b is shown in figure 5 and summarized in table 1.

The highest lattice resistance at 0 K during block-like shear $(D_1, 0, 0)$ occurs at $D_1/b = 0.5$, where the maximum of E_{POT} is $1.14 \,\mathrm{J} \,\mathrm{m}^{-2}$, a quantity also known as the unstable stacking

Table 1. The energies of one, two and three layer SFs on the $\langle 111 \rangle \{112\}$ slip system of bcc iron using a GA potential.

D_1/b	D_2/b	D_3/b	$E_{\rm POT}$ (J m ⁻²)	Max/Min	Notation
0.500	0.000	0.000	1.141	Max	γus
0.250	0.250	0.000	0.773	_	γ2SF
0.175	0.400	0.175	0.625	Min1	
0.150	0.425	0.150	0.623	Min2	γ3SF
0.275	0.275	0.275	0.871	Min3	

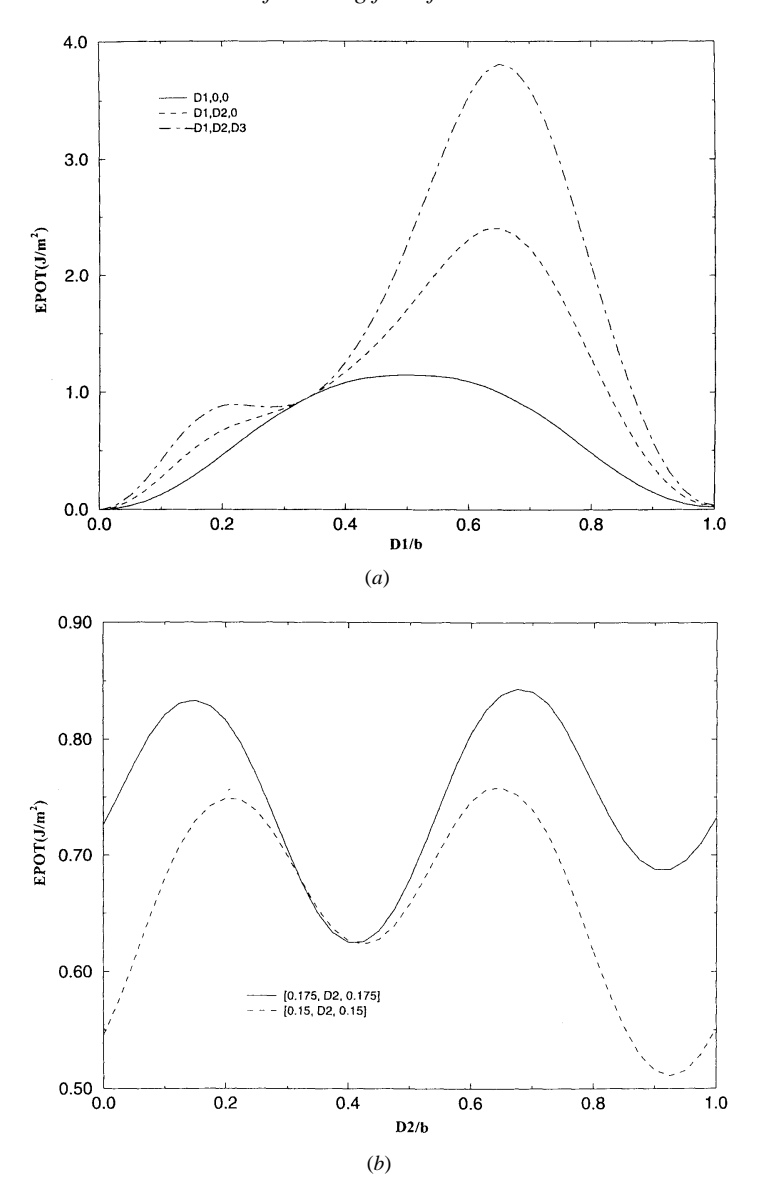


Figure 5. The change of the total potential energy in perfect samples during rigid sliding: (a) $(D_1, 0, 0)$, i.e. BLS; $(D_1 = D_2, 0)$, i.e. a particular 2SF; and $(D_1 = D_2 = D_3)$, i.e. a particular 3SF. (b) A 3SF $(0.15, D_2, 0.15)$ —showing the deepest minimum at $D_2 = 0.425$.

energy γ_{us} . According to Rice [7], this represents the energy barrier for generation of a fully developed edge dislocation on the $\langle 111 \rangle \{112\}$ slip system. There are no other energy minima for this kind of slip operation; hence, no stable intrinsic SFs exist.

A 2SF cannot be stable in the $\langle 111 \rangle \{112\}$ slip system, since there is no minimum in figure 5 for the case $(D_1, D_2, 0)$. For 3SF formation, at least two minima can be found: a local metastable higher minimum at (0.275, 0.275, 0.275) with $E_{POT} = 0.87$ J m⁻² (figure 3(*a*)), and the deepest minimum, corresponding to $E_{POT} = \gamma_{3SF} = 0.62$ J m⁻², occurring at (0.15, 0.425, 0.15) in figure 3(*b*). Table 2 shows energetics of four layer extrinsic stacking faults in the $\langle 111 \rangle$

Table 2. The energies of four layer extrinsic stacking faults in the $\langle 111 \rangle \{112\}$ slip system of bcc iron using the GA potential.

D_1/b	D_2/b	D_3/b	D_4/b	$E_{\rm POT}$ (J m ⁻²)	Max/Min	Notation
0.150	0.350	0.350	0.150	0.658	_	
0.175	0.350	0.350	0.175	0.654	Min	γ4SF
0.200	0.350	0.350	0.200	0.668	_	

{112} slip system. The minimum energy, at (0.15, 0.35, 0.35, 0.15), is $\gamma_{4SF} = 0.65$ J m⁻², which differs only slightly from the γ_{3SF} above. The results presented here using the GA potential are in agreement with Vitek's [4] analysis for the $\langle 111 \rangle \{112\}$ bcc slip system, based on several different pair potentials.

Tables 1–3 show that at temperatures near 0 K, generation of 3SF and 4SF (or multilayer twins [4]) are more favoured in the $\langle 111 \rangle \{112\}$ slip system of bcc iron compared with formation of a complete edge dislocation with relatively high unstable stacking energy. Moreover, although a stable 3SF may exist in the slip system, the transition to 4SF or to multilayer twins is probable according to the energetics in the perfect samples.

Another important characteristic of the potentials for bcc systems is the energy and stress barrier for ideal deformation twining [2, 19]. This can be modelled (figure 2(b)) by a gradual deformation of the lower part of the crystal in such a way that the first plane in the lower block is displaced by $U_1 = b/3$, the second plane by $U_2 = 2b/3$, etc, and the last plane by $U_n = nb/3$ in the $\langle 111 \rangle$ direction. In this process, the relative shear displacements of the nearest neighbouring $\{112\}$ moving planes can be described as dU = b/3 dX, where X varies from zero to unity. If X = 0.5, then U = b/6, and for X = 1 we obtain the ideal twin configuration with U = b/3, where in the lower part of the crystal we have again the ideal bcc lattice, rotated with respect to the upper (fixed) part of the crystal (figure 1). The change of the potential energy at an interior atom lying well below the twin boundary is shown in figure 6. The maximum energy barrier at the position X = 0.5 (U = b/6) corresponds to a magnitude $\gamma_{\text{twin}} = 0.236 \, \text{J m}^{-2}$. The shear stress needed for ideal deformation twinning and for BLS is given by the relation

$$\tau = dE_{POT}/dU$$

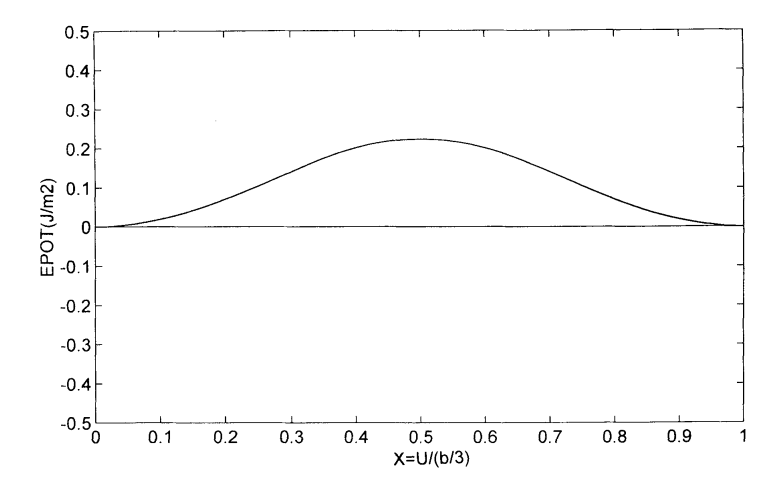
and it is presented in the lower part of figure 6 in a dimensionless form,

$$\tau^* = \tau \times constant$$

where constant = $(2\pi^2 h)/(\mu b) = 1.303 \times 10^{-10} \text{ Pa}^{-1}$ follows from the Frenkel model, $h = a/\sqrt{6}$ is the interplanar distance between {112} planes in bcc where a is the lattice parameter, and $\mu = 0.714 \text{ J m}^{-2}$ is the shear modulus in the $\langle 111 \rangle \{112\}$ slip system [3]. The peak stress in figure 6 reaches a value $\tau^*(\text{twin}) = 1.21$.

Other theoretical studies [2, 19] present the ideal shear strength in the dimensionless form τ/μ . Our value τ^* (twin) corresponds to $\tau/\mu = 0.13$, which is in very reasonable agreement with the results 0.12–0.17 presented for bcc transition metals in [2, 19].

Figure 7(a) illustrates that for BLS, the dimensionless peak stress $\tau^*(\text{disl})$ is 2.13, i.e. the lattice resistance for dislocation generation is much higher than for twin formation in the $\langle 111 \rangle \{112\}$ slip system at zero temperatures. Note that in the case of block like shear, $\mathrm{d}U = b\,\mathrm{d}X$ and U = b for X = 1.



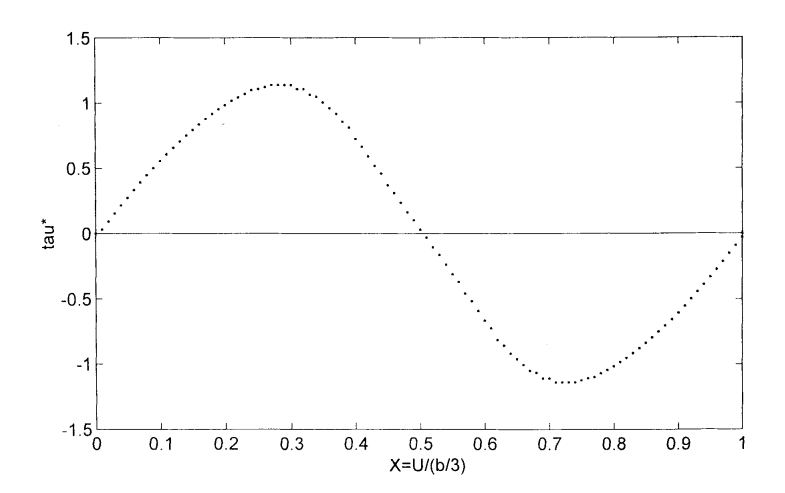


Figure 6. The change of the potential energy and the shear stress during ideal twinning at interior atoms.

3.2. Resulting forces, interplanar stress, and the work done along the slip plane for the GA potential

The GA potential used in this study is an N-body potential of the Finnis–Sinclair type [14]. The potential energy of one atom i can be written as

$$Ei = \frac{1}{2} \sum_{j} V(r_{ij}) + F(\rho_i)$$
 where $F = -A(\rho_i)^{1/2}$ and $\rho_i = \sum_{j} \phi(r_{ij})$,

and the total potential energy is $E_{POT} = \sum_{i} Ei$. Here, V is the repulsive pair potential, F represents the N-body term, ϕ is a cohesive pair potential, ρ_i is the cohesive density at the atom i, and r_{ij} is the distance between atoms i and j.

The resulting force acting at an atom k in the direction of coordinate axis x_{α} can be written as

$$R_{\alpha}(k) = \sum_{j} V_{\alpha}(k, j) + \sum_{j} (F_k + F_j) \phi_{\alpha}(k, j)$$

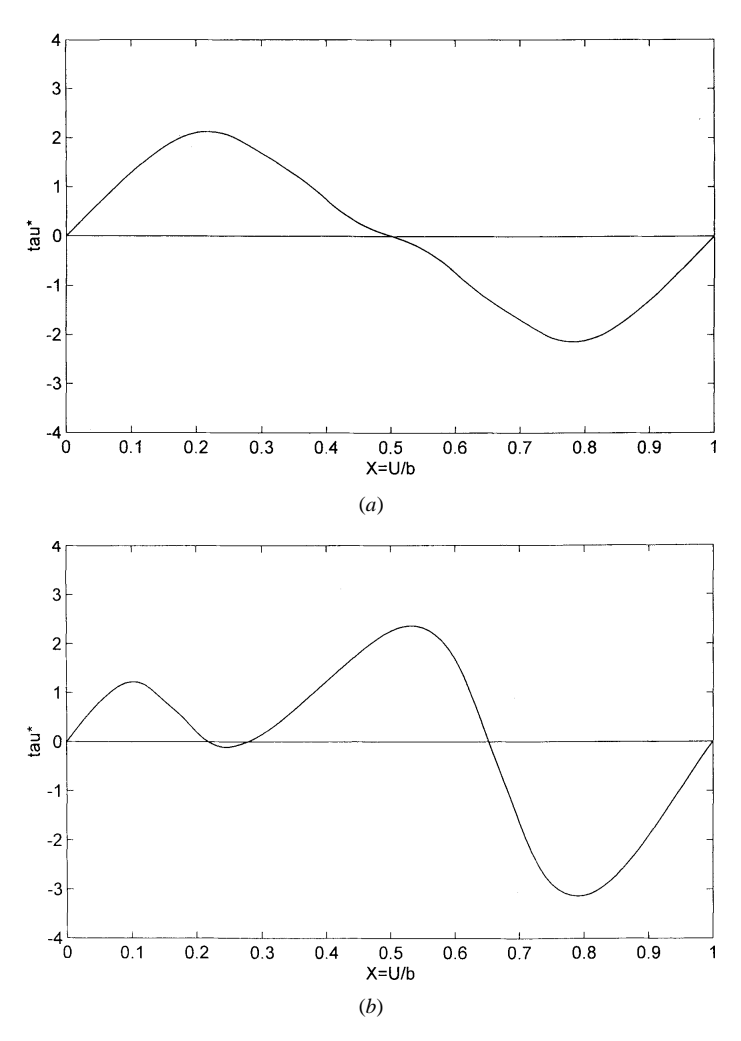


Figure 7. The shear resistance ($\tau \equiv dW_{111}/d\Delta$) during interface formation for (a) BLS with $(D_1, 0, 0)$ and (b) 3SF with $(D_1 = D_2 = D_3)$.

where $V_{\alpha} = dV/dx_{\alpha}$, $F_k = dF/d\rho_k$, and $F_j = dF/d\rho_j$. The relation for $R_{\alpha}(k)$ shows that effective pair forces

$$V_{\alpha}^{\text{eff}}(k,j) = V_{\alpha}(k,j) + (F_k + F_j)\phi_{\alpha}(k,j)$$

may be introduced formally also for the GA potential, so that according to Benedek et al's scheme [13], the interplanar forces R_{IJ} between planes I and J are $R_{IJ} \equiv R_{\alpha}(I,J) = \sum_{k,l} V_{\alpha}^{\text{eff}}(k,l)$ l > k.

$$R_{IJ} \equiv R_{\alpha}(I, J) = \sum_{k,l} V_{\alpha}^{\text{eff}}(k, l) \qquad l > k.$$

Here, atom k lies on plane I, atom l on plane J and summation is taken over all pair interactions k, l which cross the considered interplanar distance between planes I and J in the direction x_{β} of the positive normal of those planes. Interplanar stresses are then

$$R_{\alpha\beta}(I, J) = R_{\alpha}(I, J)/A_{\beta}$$

where A_{β} is the area of plane I. For the slip system $\langle 111 \rangle \{112\}$, the coordinate orientation is $x_{\alpha} = \langle 111 \rangle, x_{\beta} = \langle 112 \rangle \text{ and } x_{\alpha} \perp x_{\beta}.$

The interplanar forces and stresses can also be related only to one atom k in plane I. Then, the summation over k is ignored and A_{β} represents the area per atom in a {112} plane, i.e. $A_{\beta} = A_{112} = 2d_{110}b = a^2\sqrt{6/2}$. If plane J lies above plane I, and plane M below plane I, then the resulting force acting at atom k in plane I can be expressed via interplanar forces (per atom) as

$$R_{\alpha}(k) = R_{\alpha}(I, J) - R_{\alpha}(M, I).$$

The relations between resulting forces and interplanar stresses may be illustrated with the aid of figure 2 for BLS, 3SF, and coherent twin formation (TWIN). Here R_1 , R_2 , R_3 , R_4 , etc, denote the resulting forces acting on one atom in the plane 1, 2, 3, 4, etc, in the $\langle 111 \rangle$ direction; and R_{10} , R_{21} , R_{32} , R_{43} , etc denote corresponding interplanar shear forces between the planes 1–0, 2–1, 3–2, 4–3.

The interactions in the bcc space lattice for the GA potential are restricted to the first and the second nearest neighbours. In this framework, the range of interplanar interactions between the {112} planes is restricted to the interactions between the first and the second neighbouring planes.

In the case of BLS (figure 2(a)), the planes 1, 2, 3, 4, etc, are displaced uniquely, and $R_{32} = R_{43} = \cdots = 0$ because rigid body motion is not associated with interplanar stress in the lower part of the crystal. In the case of twinning, $R_{21} = R_{32} = R_{43} = \cdots \neq 0$, since the shear strain is homogeneous below plane 1 (figure 2(b)). If a 3SF is created according to figure 2(c), then $R_{54} = R_{65} = \cdots = 0$ in the framework of two interacting {112} planes, which means that $R_3 + R_4 = R_{32}$. Hence, the force balance at individual planes is given by the relations:

BLS:
$$R_{1} = R_{10} - R_{21} \neq 0$$

$$R_{2} = R_{21} - R_{32} = R_{21}$$

$$R_{3} = R_{32} - R_{43} = 0$$

$$R_{4} = 0$$
etc,

TWIN:
$$R_{1} = R_{10} - R_{21} \neq 0$$

$$R_{2} = R_{21} - R_{32} = 0$$

$$R_{3} = R_{32} - R_{43} = 0$$

$$R_{4} = 0$$
etc,

3SF:
$$R_{1} = R_{10} - R_{21} \neq 0$$

$$R_{2} = R_{21} - R_{32} \neq 0$$

$$R_{3} = R_{32} - R_{43} \neq 0$$

$$R_{4} = R_{43} - R_{54} = R_{43}$$

$$R_{5} = R_{54} - R_{65} = 0$$

This force balance was also verified numerically during the rigid sliding. The forces R_1 , R_2 , R_3 , R_4 , etc, created during rigid sliding in the $\langle 111 \rangle$ direction, represent internal resistance forces. The work done by these forces in the $\{112\}$ slip planes represents the energy needed to create the interface between the two blocks of the crystal, i.e. the energy for boundary formation:

BLS:
$$W_{111} = \int R_1 dU_1 + \int R_2 dU_2 = \int (R_1 + R_2) dU$$
 where $dU = b dX$

TWIN:
$$W_{111} = \int R_1 \, dU_1 = \int R_1 \, dU$$
 where $dU = (b/3) \, dX$
3SF: $W_{111} = \int R_1 \, dU_1 + \int R_2 \, dU_2 + \int R_3 \, dU_3 + \int R_4 \, dU_4$ where $R_5 = 0$.

The energy W_{111} for BLS, TWIN, and the 3SF is shown in figures 8(a)–(c). The figures illustrate that the lattice resistance during coherent twin boundary formation and for 3SF formation at (0.27, 0.27, 0.27) is smaller than during BLS.

The above equations, combined with inspection of figure 2, show that for BLS, $R_{10} = R_1 + R_2$, with $dU_{21} = 0 = \cdots = 0$; hence,

$$W_{111} = \int R_{10} \, \mathrm{d} U_{10} = W_{10}.$$

For twin formation, $R_{10} = R_1 + R_{21}$, $dU_{10} = dU_{21} = \cdots = dU$; hence,

$$W_{111} = \int (R_{10} - R_{21}) dU = W_{10} - W_{21}.$$

Finally, for 3SF formation, $dU_1 = dU_{10}$, $dU_2 = dU_{10} + dU_{21}$, $dU_3 = dU_{10} + dU_{21} + dU_{32}$; hence,

$$W_{111} = W_{10} + W_{21} + W_{32}$$

where $W_{10} \equiv \int R_{10} dU_{10}$, $W_{21} \equiv \int R_{21} dU_{21}$, and $W_{32} \equiv \int R_{32} dU_{32}$ are the respective works done by the individual interplanar stress components.

In the case of BLS and 3SF, the strain energy in the upper and lower blocks is zero, while for deformation twinning (figure 2(b)), $E_{\text{DEF}}(+) = 0$, and $E_{\text{DEF}}(-) \neq 0$. Therefore, the global energy balance can be described by the relations

BLS:
$$E_{\rm POT} = W_{111} = W_{10} = W$$
 since $E_{\rm DEF}(+) = E_{\rm DEF}(-) = 0$ and $W_{21} = 0$ TWIN: $E_{\rm POT} = W_{111} + E_{\rm DEF}(-)$

3SF:
$$E_{POT} = W_{111} = W_{10} + W_{21} + W_{32} = W$$
 since $E_{DEF}(+) = E_{DEF}(-) = 0$.

Figures 5(a) and 8, combined with the relations above, show that for BLS and 3SF, the global energy balance in the system agrees with the work done in the slip system by the resulting forces and by the interplanar stresses, i.e. $E_{\rm POT}=W_{111}\equiv W$. The history of R_{10} during BLS is identical with the shear stress $\tau={\rm d}E_{\rm POT}/{\rm d}U$ in figure 8(a), i.e. $R_{10}={\rm d}E_{\rm POT}/{\rm d}U={\rm d}W_{111}/{\rm d}U=\tau$.

The values of R_{10} and R_{21} for coherent twinning are shown in figures 9(a) and (b), together with W_{10} and W_{21} . Here, the values of R_{21} and W_{21} correspond to the global energy balance for interior atoms in figure 6, while R_{10} and W_{10} are different, which follows from the relations given above.

The critical shear stress for 3SF with $D_1=D_2=D_3$ in figure 7(b) was derived as $\tau=\mathrm{d}W_{111}/\mathrm{d}\Delta=\mathrm{d}E_{\mathrm{POT}}/\mathrm{d}\Delta$, where $\Delta=D_1+D_2+D_3=U_{10}+U_{21}+U_{32}$ is the total displacement of the lower block in figure 2(c). Since $W_{111}=W_{10}+W_{21}+W_{32}$, the shear stress τ is related to interplanar stress as

$$\tau = R_{10} dU_{10}/d\Delta + R_{21} dU_{21}/d\Delta + R_{32} dU_{32}/d\Delta$$

which represents a weighted average of the interplanar stress components.

Figures 7(a) and (b), as well as figures 6 and 9, show that the critical shear stress for ideal twinning and for 3SF generation is substantially smaller at absolute zero than the stress needed for generation of a full dislocation (figure 7(a)) in the $\langle 111 \rangle \{112\}$ slip system of a perfect bcc iron crystal; therefore, we may also expect generation of 3SF and twins at the crack tip under sufficiently large levels of applied stress. The development of an analytical model for generation of a 3SF at a crack tip is in progress [20].

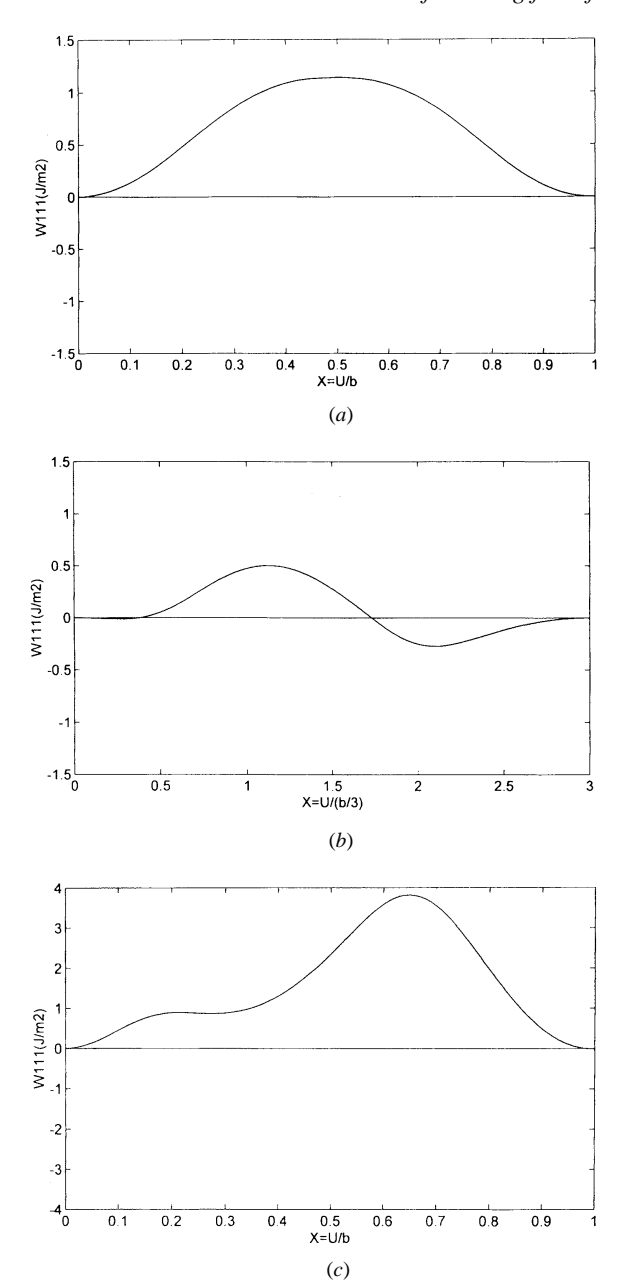
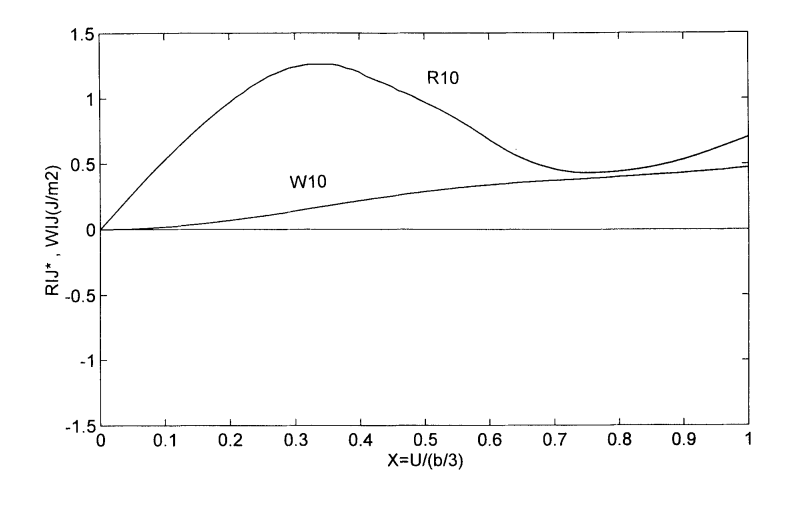


Figure 8. The work W_{111} done along slip planes by internal resistance forces acting in the individual slip planes during (a) BLS, (b) TWIN and (c) 3SF formation with $(D_1 = D_2 = D_3)$.

3.3. MD crack simulations

Previous MD simulations with medium-sized samples ($M \times N = 100 \times 50$) indicated that twin formation at a crack tip under quasistatic loading could be expected in the region of loading corresponding to an applied stress intensity factor $K_{\rm A} = 0.74-0.78 K_{\rm G}$. Here we present MD simulations in large samples (400×200), where we avoid a possible influence of waves emitted from the crack tip due to bond breakage and reflected back to the crack tip (back wave reflections). We map existing interactions at each time step, and we know the velocities of longitudinal and shear waves in our model [3], as well as sample dimensions.



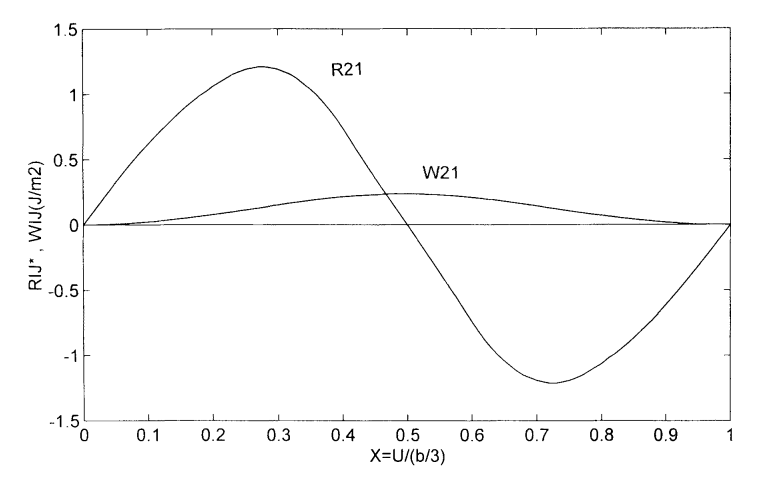


Figure 9. The histories of R_{10} , W_{10} , R_{21} , and W_{21} during formation of an ideal CT boundary.

Table 3. Relative shear displacements $U_{IJ}(T)$ at the crack tip and at interior atoms U_{IJ} in MD simulation with $l_0=20d_{110}$ under $\sigma_{\rm A}=0.78\sigma_{\rm G}$. Δ denotes the total shear displacement.

Number	$U_{10}(\mathrm{T})/b$	$U_{21}(\mathrm{T})/b$	$U_{32}(T)/b$	$\Delta(\mathrm{T})/b$	U_{10}/b	U_{21}/b	U_{32}/b	U_{43}/b	Δ/b
4000	0.260	0.177	0.079	0.516	0.172	0.126	0.049	0.029	0.348
4500	0.263	0.183	0.087	0.533	0.177	0.136	0.054	0.026	0.367
5000	0.279	0.211	0.102	0.592	0.202	0.183	0.077	0.019	0.462
5200	0.333	0.320	0.172	0.825	0.257	0.312	0.143	0.008	0.712
5250	0.326	0.370	0.310	1.006	0.273	0.349	0.299	0.114	1.030
5300	0.368	0.351	0.347	Twin	0.308	0.335	0.337	0.246	Twin
5350	0.391	0.349	0.344	Twin	0.336	0.336	0.328	0.330	Twin
5368	Back wave reflections								

The following section shows that transformation from a 3SF to a twin at the crack tip occurs below the Griffith stress for short cracks under quasistatic loads and it may cause elementary crack advance, unimpeded by the reflected stress waves.

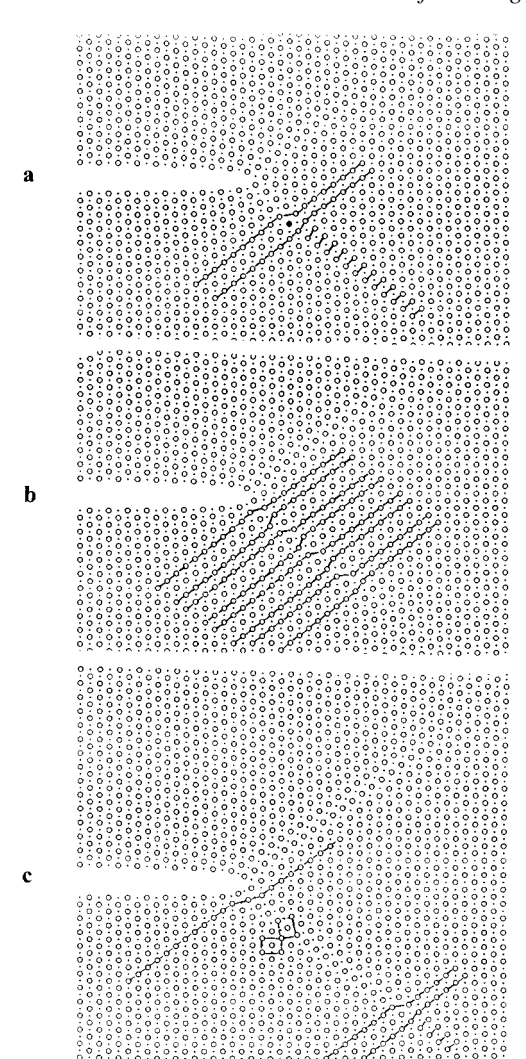


Figure 10. Atomic configuration in MD crack simulation under $\sigma_{\rm A}=0.78\sigma_{\rm G}$ at various time integration steps equal to (a) 5000, (b) 5200 and (c) 5250; $l_0=20d_{110}$.

3.3.1. Short crack, higher applied stress. The applied stress $\sigma_{\rm A}=0.78\sigma_{\rm G}$ for a half crack length $l_0=20d_{110}$ corresponds to a stress intensity factor $K_{\rm A}=0.78K_{\rm G}$, where $K_{\rm G}=C(2\gamma)^2=\sigma_{\rm G}(\pi l_0)^{1/2}$. Table 3 presents the relative shear displacements at the crack tip (index T) and at interior atoms (without index) at the time integration steps when graphic output was generated. Details of the atomic configuration at the crack tip are shown in figures 10(a)-(c). The open circles and dots in figure 10 denote a different position of the atoms projected into a (110) plane with respect to the normal $x_3=[110]$. Table 3 and figures 10(a)-(c) show that up to the 5000th time step, the configuration represents a partial dislocation with Burgers vector $\approx b/2$, with a 2SF trailing behind the dislocation. After step 5000, a 3SF is developed in the $\langle 111 \rangle \{112\}$ slip system. The 3SF is clearly visible in figure 11(a) at time step 5200, where the same notation (dots) is used for all the atoms. The 3SF is of extrinsic type and it may be interpreted as an emission of three partial dislocations from the crack tip in the individual planes 1, 2, and 3 with $b_1=U_{10},b_2=U_{21}$ and $b_3=U_{32}$.

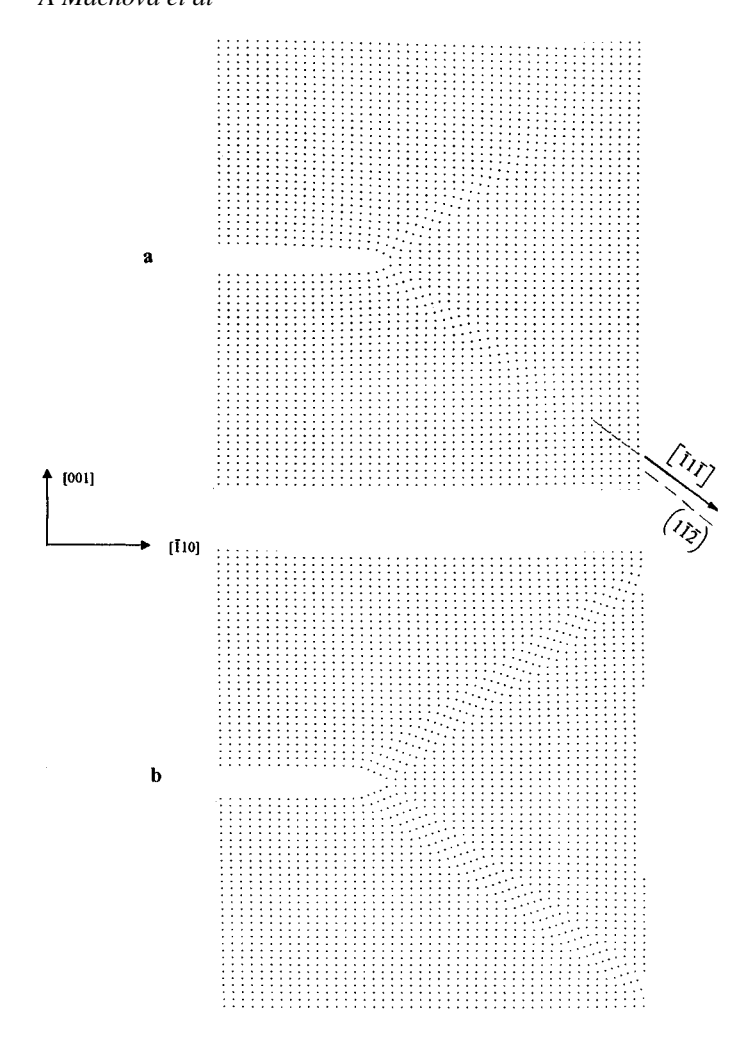


Figure 11. Extrinsic SFs at the crack tip of the crack $l_0 = 20d_{110}$ under $\sigma_A = 0.78\sigma_G$: (a) the unstable 3SF at time step 5200 and (b) twins at time step 5350.

Table 3 shows that when the total displacement Δ reaches the value of b, twin transformation occurs, as is shown in figures 10(c) and 11(b). The transformation is visible also in figures 12(a) and (b), where the time development of the relative shear displacements and of the interplanar stresses at interior atoms is shown. It begins at around step 5200, where the U_{43} component starts to increase rapidly. This indicates a transition to 4SF and subsequently to a multilayer twin. The transition is not caused by the back wave reflections mentioned in section 1 (which is denoted in figures 12, 13, and 15 by vertical dashed lines). The first reflected waves may arrive back at the crack tip at step 5368. Figure 13 shows that the interplanar stress $R_{10}(T)$ at the crack tip does not vanish, unlike the other components. This is perhaps related to the existence of a stress gradient at the crack tip, leading to $U_{10}(T) > U_{21}(T)$.

The dependences R_{IJ} against time (t) and U_{IJ} against t can be replaced by the stress–displacement curves shown in figures 14(a) and (b). Figure 14(a) shows that the behaviour of $R_{10}(T)$ is similar to R_{10} in figure 9(a) during generation of the CT boundary by rigid sliding. This indicates that the interplanar stress $R_{10}(T)$ does not enable generation of the

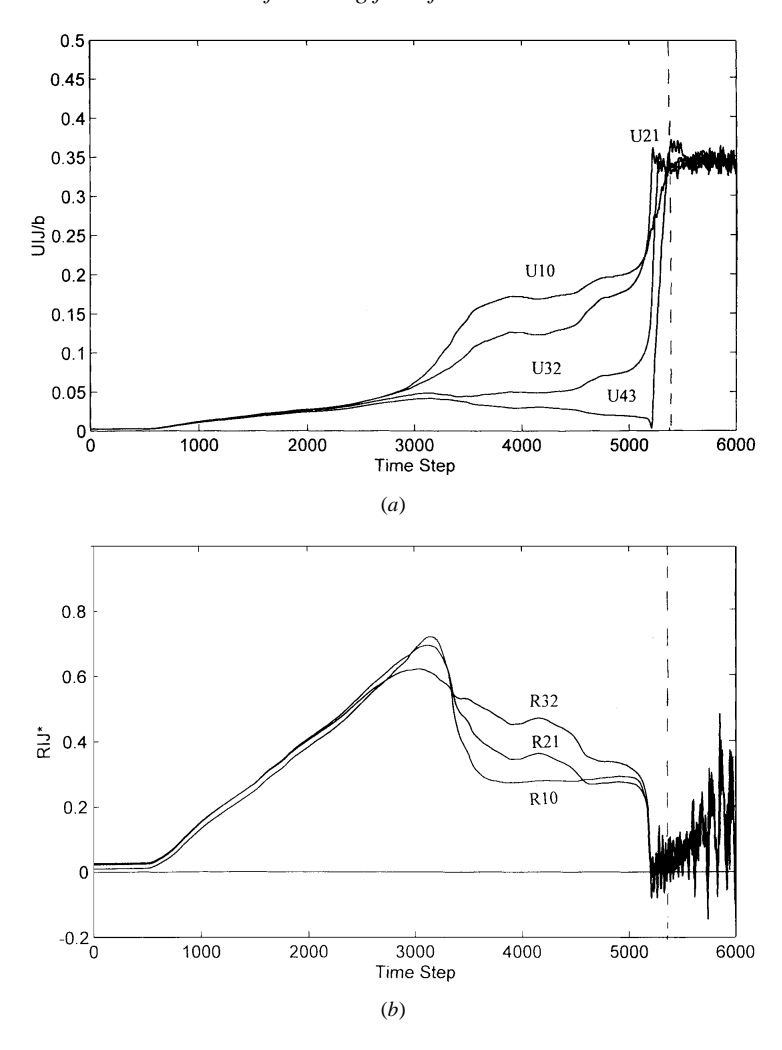


Figure 12. Time development of (a) relative shear displacements and (b) interplanar stresses at interior atoms in MD simulation with $\sigma_A = 0.78\sigma_G$ and $l_0 = 20d_{110}$.

stable 3SF with $\gamma_{3SF} = 0.62$ J m⁻². Although the interior atoms may be driven to the stable 3SF, the stress conditions at the crack tip, namely $R_{10}(T)$, cause the transition to twin formation (figure 10(c)).

The work $W = W_{10} + W_{21} + W_{32}$ done by the interplanar stresses at the crack tip up to step 5200 (when $R_{21}(T)$ and $R_{32}(T)$ vanish) is $W_T = 0.507$ J m⁻², while at interior atoms W = 0.457 J m⁻². This indicates that when W_T reaches or exceeds the $W_{111} = 0.5$ J m⁻² (figure 8(*b*)) needed for the creation of the ideal CT boundary, a transformation from 3SF to TWIN may start from the crack tip, as observed in the MD simulation.

The work W needed for the transformation 3SF \rightarrow TWIN in the MD simulations is smaller than E_{POT} for (0.25, 0.35, 0.15) following from rigid sliding in the perfect samples. Also, the peak stresses in the MD simulations are lower by about 30% than the critical shear stress for ideal twinning shown in figure 6. This could possibly be explained by the findings from Sun *et al* [21] that normal relaxation in slip systems may decrease the energy and the peak stresses needed for shear processes at the crack tip. The normal relaxations were also

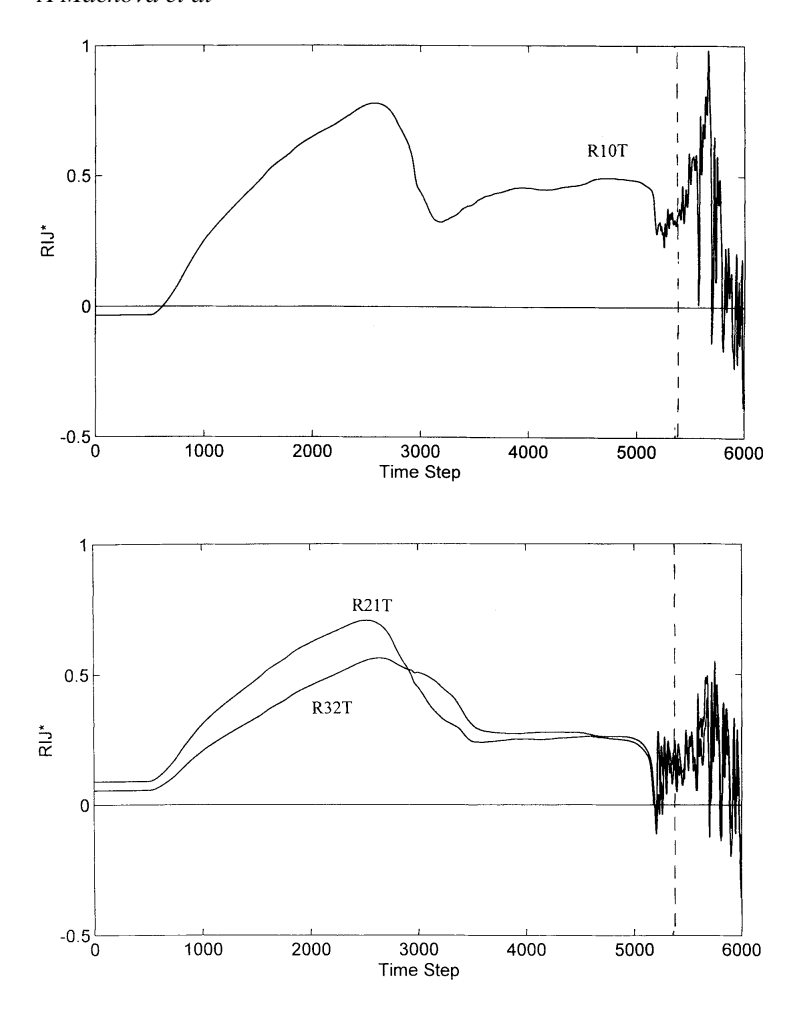


Figure 13. Interplanar stresses at the crack tip during quasistatic loading up to $\sigma_A = 0.78\sigma_G$ and $l_0 = 20d_{110}$.

found by Bristowe $et\ al\ [5]$ to play an important role in the energetics of shear processes on $\{112\}$ planes in iron.

Figure 15 shows the global energy balance for the sample $M \times N = 400 \times 200$. It is obvious that up to time step 5200, the kinetic energy $E_{\rm KIN}$ in the system is very small. This means that external loading is really quasistatic, and that the average temperature T (estimated from the Boltzmann equation $E_{\rm KIN}/N_a = k_{\rm B}T$ for two degrees of freedom, where N_a is the total number of atoms and $k_{\rm B}$ is Boltzmann's constant) in the whole sample is close to 0 K. Generation of a 3SF at the crack tip increases the total potential energy in the system. When the individual stress components R_{IJ} reach the first zero values, $E_{\rm POT}$ at step 5200 reaches a maximum. After the transformation to a twin band, wherein strain energy is zero, $E_{\rm POT}$ begins to decrease and $E_{\rm KIN}$ increases since the transition is very rapid (see figure 12(a)).

Mapping the local potential energies E_i in the shear band shows that the transformation 3SF \rightarrow TWIN occurs when the local energies on planes 1 and 2 (figure 4) at the crack tip exceed the energy barrier for ideal twinning (figure 6). The velocity of the twin transformation

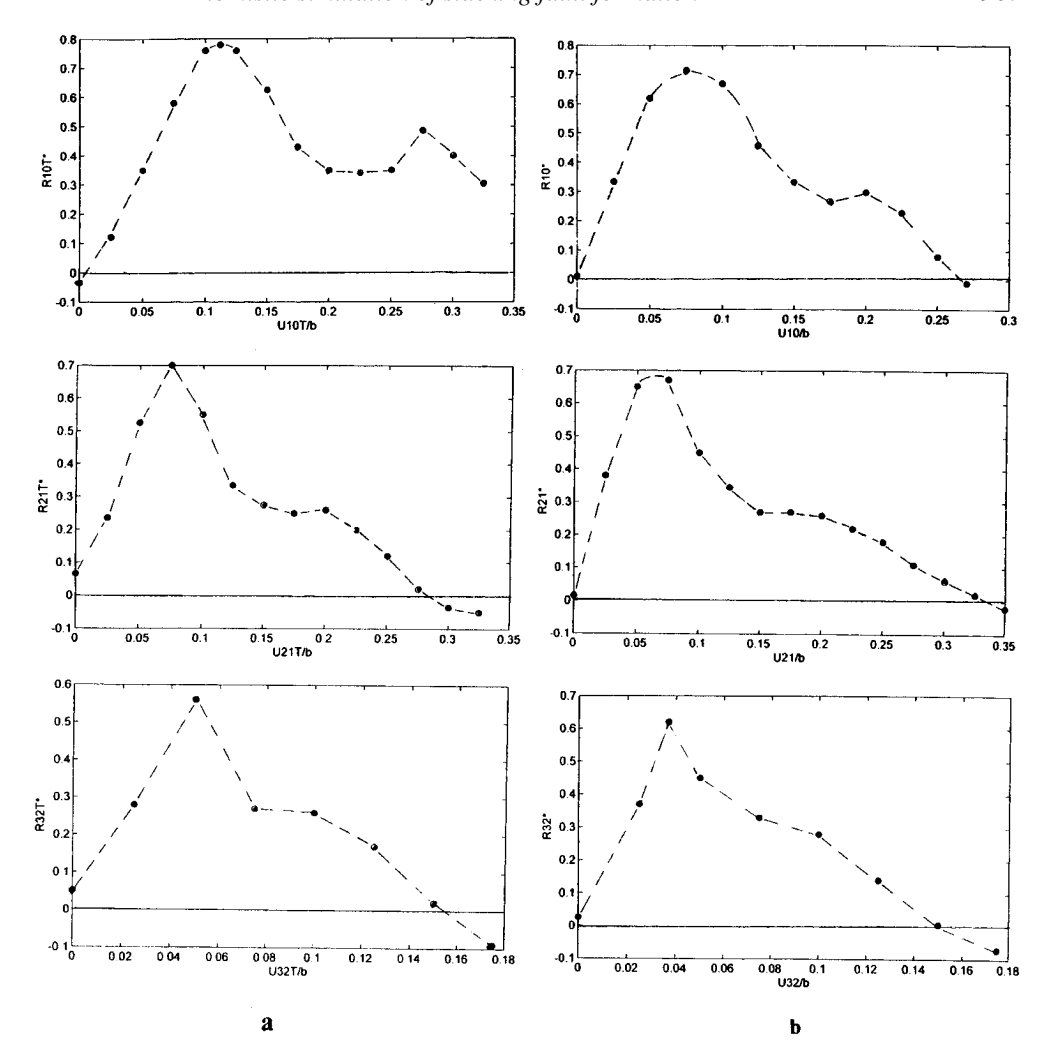


Figure 14. The shear against displacement curves from MD simulation with $\sigma_A = 0.78\sigma_G$ and $l_0 = 20d_{110}$: (a) at the crack tip and (b) at interior atoms.

 dU_{43}/dt corresponds to about 53 m s⁻¹, which means a transient increase of the local kinetic energies and of a local temperature per one atom in the shear band by about 10 K.

In accordance with isotropic linear elastic fracture mechanics (LFM), the strain energy in the $\langle 111 \rangle \{112\}$ slip system needed for formation of the unstable 3SF with $U_{10}=0.25$, $U_{21}=0.35$, $U_{32}=0.15$ at step number = 5200 may be estimated as

$$W(LFM) = \int_0^{D'} \tau(K_A) \, dU$$

where $D = U_{10} + U_{21} + U_{32} = 0.75b$ and $\tau(K_{\rm A}) = 0.235K_{\rm A}/(2\pi3b)^{1/2}$ for the angle $\theta = 35^\circ$ and r = 3b. For $K_{\rm A} = 0.78K_{\rm G}$ we obtain a value

$$W(LFM) = \tau(K_A)D = 0.432 \text{ J m}^{-2}$$

which is very close to $W(MD) = 0.457 \text{ J m}^{-2}$ for interior atoms in the MD simulations. Alternatively, using W(MD) and the LFM relations, we may obtain the critical stress intensity

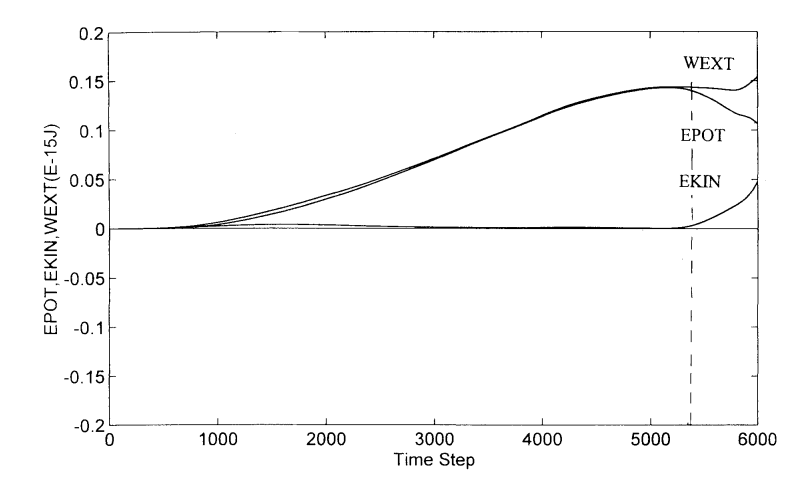


Figure 15. The global energy balance in MD simulation during quasistatic loading up to $\sigma_{\rm A}=0.78\sigma_{\rm G}$ and $l_0=20d_{110}$.

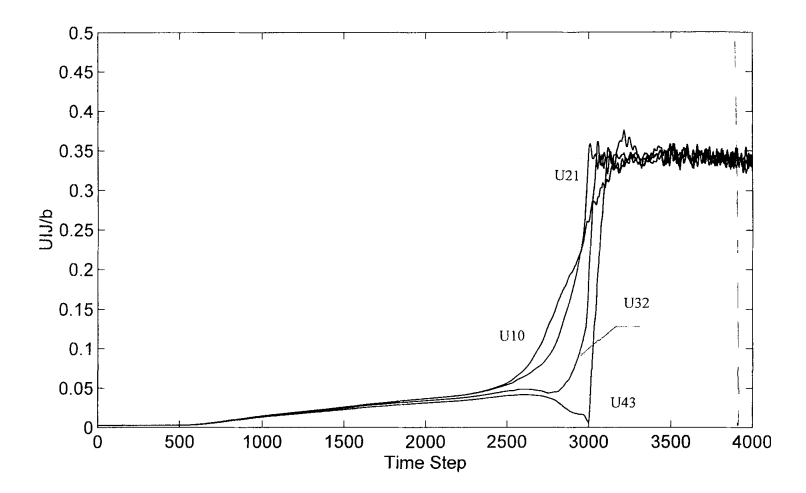


Figure 16. Time development of relative shear displacements at interior atoms in MD simulation with $\sigma_A = \sigma_G$ and $l_0 = 20d_{110}$.

needed for the generation of the unstable 3SF and subsequent transformation 3SF \rightarrow TWIN. This gives $K_A = 0.82 K_G$, which is in good agreement with our MD results.

Under a faster load rate, when $\sigma_A = \sigma_G$ in the plateau region in figure 3, the transformation from a 3SF to a multilayer twin has been observed even during the linear phase of loading at time step 3000. At this moment, the applied load corresponds to $\sigma_A(t) = \frac{3}{4}\sigma_G$ and to $K_A \approx 0.75 K_G$. The first bonds towards the second neighbours were broken at the crack tip at time step 2843. The first back wave reflections do not become a factor at the crack tip until time step 3875. The histories of $R_{IJ}(T)$, R_{IJ} , $U_{IJ}(T)$ and U_{IJ} are similar in character to the previous case, but time development of plastic relaxation at the crack tip is more rapid. The stresses reach peak values in the time interval 2200–2500. In figure 16, the generation of unstable SFs and their subsequent transformation to twins is shown to be realized in a short time interval 2500–3000, while in the previous case it was in the interval 3000–5200. The faster loading enables us to delay the influence of reflected stress waves from the time of

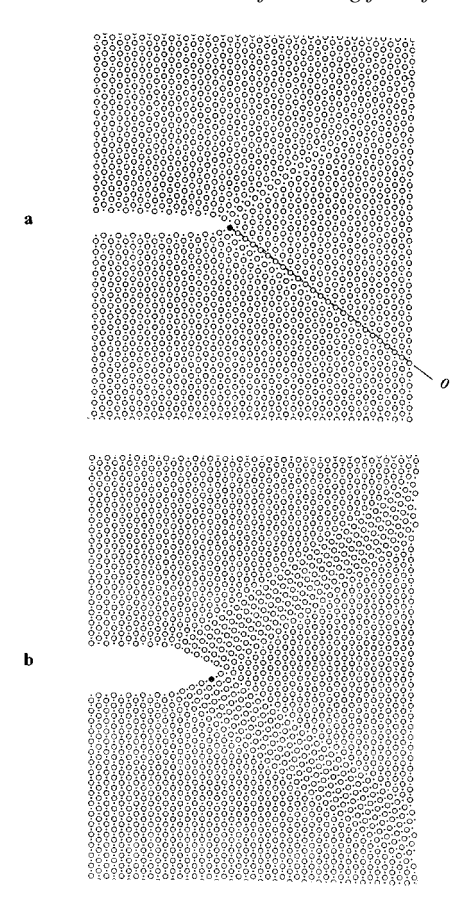


Figure 17. Atomic configurations near the crack tip in MD simulation during quasistatic loading of the crack $l_0 = 20d_{110}$ up to $\sigma_A = \sigma_G$: (a) time step 3000 and (b) time step 3500.

the transformation 3SF \rightarrow TWIN and to observe unimpeded crack advance after twinning below K_{G} .

Atomistic configurations near the crack tip at time steps 3000 and 3500 are shown in figures 17(a) and (b). Figure 17(a) shows an unstable 3SF with vanishing shear stress inside the slip band (illustrated by the dislocation dipoles in figure 10(b)). Figure 17(b) shows the situation after the transformation, when the twin extends above the border plane 0 (denoted in figures 4 and 17(a)), and the original crack tip atom (denoted in black) appears at the free crack surface. This represents an elementary crack advance due to twinning. At this moment, $R_{10}(T)$ vanishes, since the atom lies inside the twin band. The crack tip bond may be broken when the shear displacement of plane 0 reaches $U_0 \approx 2b/3$. Then, the separation of the crack tip atoms exceeds the cut-off radius $r_c = 1.31a$ of the GA potential and shear bond breaking occurs. This happens before wave reflections from previous bond breakage influence the crack tip and also before the fast twinning reaches the sample borders, as shown in figure 18 (where only part of the whole sample is shown). This mechanism of crack growth is similar to a twin intersection model proposed by Müllner [22] to explain brittle–ductile transition in austenitic steel observed experimentally at low temperatures. Twins were observed in this case even at 4 K [23].

Our results indicate that crack advance may be caused by twinning at the crack tip—relevant when microcracks are under a relatively large applied stress at low (average)

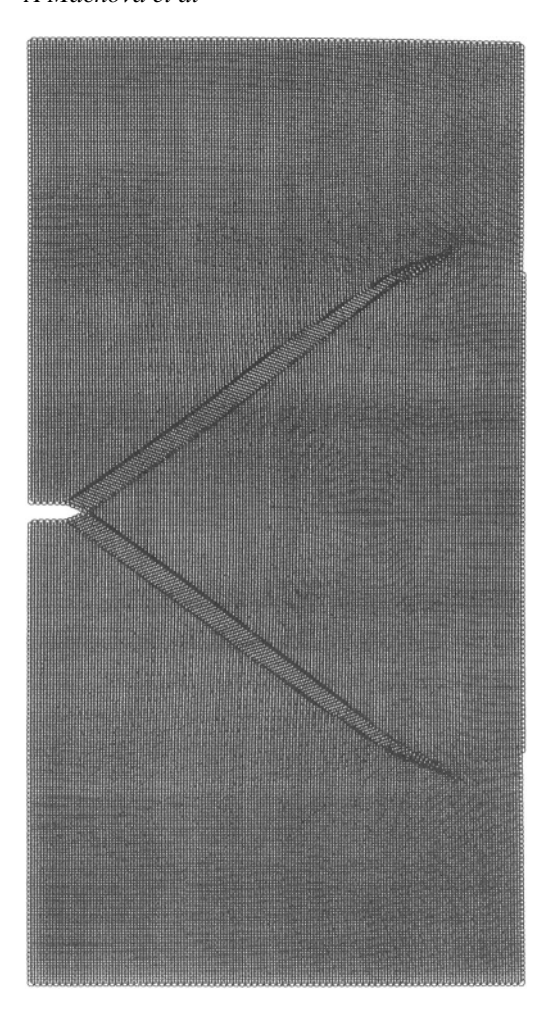


Figure 18. Atomic configuration in a larger part of the sample during quasistatic loading up to σ_G at time step 3500; $l_0 = 20d_{110}$.

temperatures. This could be a possible explanation of the experimental observation that twinning stress also represents fracture stress in bcc crystals at low temperatures [1].

The stability of defects generated at crack tips may be examined in atomistic simulations, also via computer experiments of loading–unloading [24]. We have performed these experiments in medium samples ($M \times N = 100 \times 50$), $l_0 = 20 d_{110}$, where the same processes under quasistatic loading have been observed as in the large-scale simulations presented in this section. When gradual unloading (equivalent to a linear loading phase) begins near the maximum of the potential energy in the system (and before arrival of the back wave reflections at the crack tip), the 3SF \rightarrow TWIN transformation is observed during the unloading phase, leading to an extensively twinned structure under no external loading. If unloading commences *before* the unstable 3SF arises from the partial dislocation with 2SF behind it (i.e. well below the maximum of $E_{\rm POT}$), then unloading leads to the disappearance of the incipient defects at the crack tip.

3.3.2. Longer crack, lower applied stress. In this case, the half crack length is $l_0=80d_{110}$ and the applied stress $\sigma_A=0.71\sigma_G=0.274\times 10^{10}~N~m^{-2}$ is relatively low compared with our

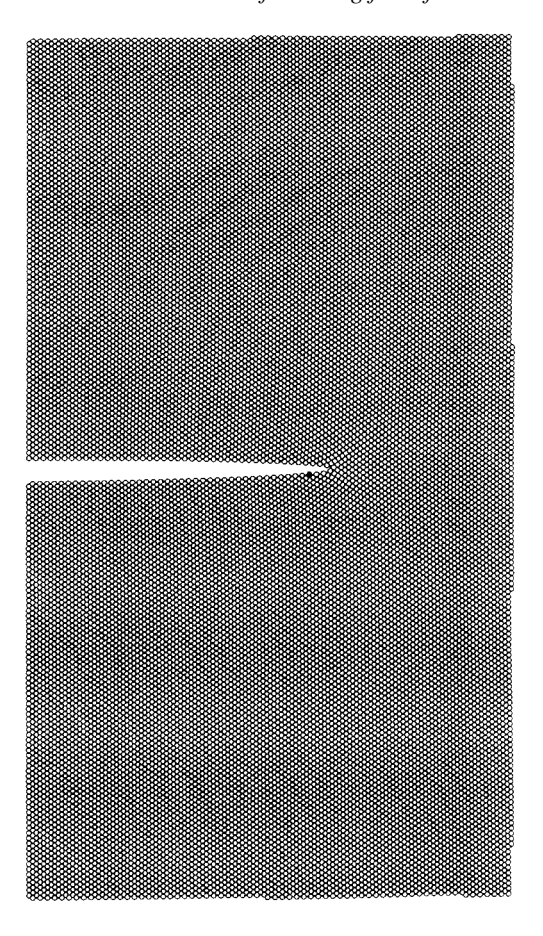


Figure 19. Brittle crack initiation of the longer crack $l_0 = 80d_{110}$ at time step 4500 and $K_A = K_G$.

previous cases and it lies in the elastic regime of the theoretical uniaxial tension curve for the GA potential in [3]. Similarly, the applied shear stress $\tau_A = 0.47\sigma_A$ (defined as the resolved shear stress on planes inclined at 35° in remote locations from the crack, determined with a Schmid factor of 0.47) lies in the elastic region of the theoretical shear–displacement curve shown in figure 6. The corresponding stress intensity factor is $K_A = F_I \sigma_A (\pi l_0)^{1/2} = K_G$; note the stress intensification $F_I = 1.4 = (0.71)^{-1}$ [25] caused by the finite geometry of our samples ($M \times N = 400 \times 200$), whereas for $l_0 = 20d_{110}$, $F_I \approx 1.0$.

In each of our crack geometries, the active $\langle 111 \rangle \{112\}$ slip systems begin at the crack tip and terminate at the free external (-110) sample border. In addition to the different crack lengths and Griffith stress, another important difference between sections 3.3.1 and 3.3.2 is the boundary correction factor $F_{\rm I}$ for $l_0=20d_{110}$ and $80d_{110}$. The larger value of $F_{\rm I}$ for $l_0=80d_{110}$ enables us to decrease the applied stress required for crack initiation at $K_{\rm A}=K_{\rm G}$, as follows from the above relation.

Figure 19 shows that at the Griffith level $K_A = K_G$, the crack initiated (the full circle represents the original crack tip atom) in agreement with the expectation according to linear elastic fracture mechanics. Under a slightly smaller applied stress, $\sigma_A = 0.67\sigma_G$, i.e. for $K_A < K_G$, the crack $l_0 = 80d_{110}$ was stable. Under the critical loading $K_A = K_G$, the crack was initiated when the total potential energy in the system exceeded the expected Griffith level.

Although crack initiation was accompanied by some shear processes localized only in the vicinity of the crack tip, the defects disappear after crack advance, as may be seen in figure 19. Twin generation is not observed, and crack extension has a brittle character. This can be explained by the fact that incipient defects are restricted to the stressed crack tip region (see, e.g., figure 12 prior to time step 5000). When the original crack tip atoms become 'surface atoms' subsequent to crack advance, they are unloaded, and the unstable defects vanish, similar to the unloading experiments mentioned in section 3.3.1.

Comparison of the cases $l_0 = 20d_{110}$ and $l_0 = 80d_{110}$ clearly indicates that the applied shear stress τ_A plays an important role in twin formation. The critical level of τ_A may be estimated similarly as in section 3.3.1:

$$\int_0^D \tau_{\rm A} \, dU = W(\text{MD}) = 0.457 \,\text{J m}^{-2} \qquad D = 0.75b$$

which gives $\tau_A(\text{crit}) = 0.25 \times 10^{10} \,\text{N m}^{-2}$. For $l_0 = 20d_{110}$, the applied shear stress is higher, $\tau_A = 0.28 \times 10^{10} \,\text{N m}^{-2}$, which enables the extension of the unstable 3SF up to a distance $r \approx 11b$ from the crack tip (figure 10(b)). For $l_0 = 80d_{110}$ at $K_A = K_G$, the contribution $\tau(K_A, r, \theta)$ from the expected asymptotic linear elastic stress field decreases below $\tau_A(\text{crit})$ for r > 4b and the small nominal shear stress $\tau_A = 0.13 \times 10^{10} \,\text{N m}^{-2}$ does not enable development of the unstable 3SF and subsequent twin transformation. In other words, even though the near tip field (for a given K_A) is expected to be similar in each of our geometries, the stress field further away is less intense when $l_0 = 80d_{110}$. This explains qualitatively our different results for $l_0 = 80d_{110}$ against $l_0 = 20d_{110}$.

4. Summary

- (1) Interplanar stresses for the GA potential (*N*-body potential of the Finnis–Sinclair type) can well describe the local force balance at slip bands and also the global energy balance in the system. These stresses, as well as global energy balance concepts, have been used to examine the stability of extrinsic SFs in bcc iron in perfect crystals, as well as in cracked crystals loaded quasistatically in mode I.
- (2) The global energy balance performed with the GA potential in the perfect samples agrees with Vitek's results [4] that stable extrinsic 3SFs may theoretically exist in the (111){112} slip systems of bcc iron. The energy barrier between 3SFs and 4SFs is very small, so the transition from a 3SF to a multilayer incoherent twin is probable. Since the unstable stacking energy for formation of a complete dislocation is larger than the lattice resistance for the formation of a 3SF, generation of a 3SF at a loaded crack tip and subsequent transformation to a multilayer twin is probable.
- (3) Molecular dynamic crack simulations using the GA potential under quasistatic loading in mode I show that the stress intensity required for generation of extrinsic SFs in the $\langle 111 \rangle \{112\}$ slip systems from the crack tip of a central (001)[110] crack lies below σ_G for a half crack length $l_0 = 20d_{110}$, where d_{110} is the interplanar distance between neighbouring $\{110\}$ planes. The loading level agrees well with an estimate according to isotropic linear elastic fracture mechanics. The process begins as the formation of an incipient partial edge dislocation (with Burgers vector approximately b/2) from the crack tip, with an unstable 2SF trailing the dislocation. This causes partial relaxation of the interplanar shear stresses in the slip system. The 2SF is gradually transformed to an extrinsic 3SF, leading to vanishing stresses inside the slip band and to a maximum of the total potential energy in the system. The interplanar stress at the crack tip cannot decrease to zero, and its development has a character similar to that during formation of an ideal CT boundary.

When the work done by the interplanar stresses at the crack tip exceeds the energy needed for formation of a CT boundary, a very fast transition of the unstable 3SF to a multilayer twin is observed in the MD simulations. This indicates that the stress gradient at the crack tip does not enable the minimum 3SF energy to be reached with the symmetric distribution of relative shear displacements presented in table 3. Transformation to multilayer twins decreases the total potential energy in the system, since the strain energy inside the twin band is zero. When twins extend above the original boundary, an elementary crack advance is observed, facilitated by twinning at the crack tip. These processes are not influenced by back wave reflections from previous bond breakage in the slip system. The peak shear stresses in the MD simulations lie below the peak stress needed for ideal twinning by about 30%.

(4) The results from our atomistic simulations under quasistatic loading suggest a possible mechanism for how twins may evolve from partial dislocations distributed in three adjacent {112} planes. This mechanism closely follows original suggestions of Ogawa [1], based on his experimental results. The MD results support the experimental findings that twinning and fracture at low temperatures in bcc iron are cooperating processes and that fracture may be initiated by twinning, when sufficient stress intensity for twin formation may appear at the crack tips during external loading. The results support other experimental observations that the stress required for twinning may be regarded as fracture stress in bcc crystals.

Acknowledgments

The work was supported by the Grant Agency AS CR in Prague under contract A-2076701, by a CR-USA grant (KONTAKT 058), as well as the National Science Foundation (USA) under grant INT-9707863. The authors thank Dr F Kroupa for valuable comments and discussions. GEB would like to acknowledge discussions with Michael Ortiz and Alexei Romanov.

References

- [1] Ogawa K 1965 Edge dislocations dissociated in {112} planes and twinning mechanism of b.c.c. metals *Phil.*
- [2] Wei Xu and Moriarty J A 1996 Atomistic simulation of ideal shear strength, point defects, and screw dislocations in bcc transition metals: Mo as a prototype Phys. Rev. B 54 6941
- [3] Machová A and Ackland G J 1998 Dynamic overshoot in alpha-iron by atomistic simulations Modelling Simul. Mater. Sci. Eng. 6 521
- [4] Vitek V 1970 Multilayer stacking faults and twins on (211) planes in b.c.c. metals Scr. Metall. 4 725
- [5] Bristowe P D, Crocker A G and Norgett M J 1974 The structure of twin boundaries in body centered cubic materials J. Phys. F: Met. Phys. 4 1859
- [6] Rice J R and Thomson R 1974 Ductile versus brittle behaviour of crystals *Phil. Mag.* **29** 73
- [7] Rice J 1992 Dislocation nucleation from a crack tip: an analysis based on the Peierls concept J. Mech. Phys. Solids 40 239
- [8] Mullins M 1984 Computer simulation of fracture using long range pair potentials Acta Metall. 32 381
- [9] Cheung J K and Yip S 1994 A molecular-dynamics simulation of crack-tip extension: the brittle-to-ductile transition Modelling Simul. Mater. Sci. Eng. 2 865
- [10] Shastry V and Farkas D 1996 Molecular statics simulation of crack propagation in α-Fe using EAM potentials Mater. Res. Soc. Symp. Proc. 409 75
- [11] Hu S Y, Ludwig M, Kizler P and Schmauder S 1998 Atomistic simulations of deformation and fracture of alpha-Fe Modelling Simul. Mater. Sci. Eng. 6 567
- [12] Ackland G J, Bacon D J, Calder A F and Harry T 1997 Computer simulation of point defect properties in dilute Fe-Cu alloy using a many-body interatomic potential *Phil. Mag.* A 75 713

- [13] Benedek G, Boffi S, Caglioti G and Bilello J C 1975 Surface energy for brittle fracture of alkali halides from lattice dynamics Surf. Sci. 48 561
- [14] Finnis M W and Sinclair J F 1984 A simple empirical N-body potential for transition metals *Phil. Mag.* A **50** 45
- [15] Alber I, Bassani J L, Khantha M, Vitek V and Wang G J 1992 Grain boundaries as heterogeneous systems: atomic and continuum elastic properties *Phil. Trans. R. Soc.* A 339 555
- [16] Lutsko J F 1989 Generalized expressions for the calculation of elastic constants by computer simulation J. Appl. Phys. 65 2991
- [17] Mullins M and Dokainish M A 1982 Simulation of the (001) plane crack in alpha-iron employing a new boundary scheme Phil. Mag. A 46 771
- [18] Kohlhoff S, Gumbsch P and Fischmeister H F 1991 Crack propagation in bcc crystals studied with a combined finite-element and atomistic model *Phil. Mag.* A 64 851
- [19] Paxton A T, Gumbsch P and Methfessel M 1991 A quantum mechanical calculation of the theoretical strength of metals *Phil. Mag. Lett.* 63 267
- [20] Beltz G E, Chang M and Machová A 1999 work in progress
- [21] Sun Y, Beltz G E and Rice J R 1993 Estimates from atomic models of tension-shear coupling in dislocation nucleation from a crack tip *Mater. Sci. Eng.* A **170** 67
- [22] Müllner P 1997 On the ductile to brittle transition in austenitic steel Mater. Sci. Eng. A 234 94
- [23] Müllner P 1997 Private communication
- [24] Cleri F, Yip S, Wolf D and Phillpot S R 1997 Atomic-scale mechanism of crack-tip plasticity: dislocation nucleation and crack-tip shielding *Phys. Rev. Lett.* 79 1309
- [25] Murakami Y 1987 Stress Intensity Factor Handbook vol 1 (Oxford: Pergamon) p 67